IL NUOVO CIMENTO **41 C** (2018) 113
DOI 10.1393/ncc/i2018-18113-9

COMMUNICATIONS: SIF Congress 2017

Multivariate Empirical Mode Decomposition analysis of Swarm data

T. ALBERTI(*)

INAF-Istituto di Astrofisica e Planetologia Spaziali - via del Fosso del Cavaliere 100, 00133 Roma, Italy

received 30 January 2018

Summary. — The magnetosphere and the ionosphere of the Earth are populated by different current systems with well-structured spatial patterns. In this paper, by using low-resolution (1 Hz) Swarm A data, we present an application of the Multivariate Empirical Mode Decomposition (MEMD) to the external variations of the geomagnetic field, allowing us to identify magnetospheric and ionospheric current systems patterns. By using both quiet and disturbed periods, we show that MEMD is able to clearly discern between magnetospheric and ionospheric contributions, evidencing magnetospheric ring current pattern, field aligned currents, ionospheric Solar quiet (Sq) and equatorial electrojet (EEJ) currents, with well-defined spatial patterns, in addition to which we observe both short- and large-scale contributions.

1. – Introduction

The geomagnetic field, as observed on the ground or by low-Earth orbiting (LEO) satellites, is the sum of contributions from many different sources, both internal and external with respect to the Earth's surface. The main part of the Earth's magnetic field is related to a self-sustaining dynamo operating in the fluid outer core, which accounts for more than 90% of the total field. Another important contribution of the internal origin is due to the magnetized lithosphere, while external origin contributions are mainly related to electric currents flowing in the ionosphere, magnetosphere and oceans [1]. The resulting magnetic field is highly variable in time and space, with temporal variations occurring on timescales ranging from milliseconds to millions of years. Particularly, the slower changes (from a year up to millions of years) are generally referred to as the geomagnetic secular variation and are related to changes in the magnetic field of internal origin. Conversely, the short-term variations are mainly associated with changes in the

(*) E-mail: tommaso.alberti@inaf.it

ionospheric and magnetospheric current systems [2]. Thanks to high quality satellite and ground magnetic data now available, different models of the geomagnetic field have been developed and improved pushing them to higher resolution in both space and time. Typical geomagnetic models are the IGRF, CHAOS, GRIMM and POMME series. However, it has been recognized that accurate modelling of the Earth's core and crustal field requires accounting for external field sources and consequently further improvement of geomagnetic models requires a better understanding of these sources. In order to distinguish between the different sources and separate different contributions to the measured magnetic field the use of advanced modelling techniques is required.

The purpose of this paper is to present an application of the Multivariate Empirical Mode Decomposition (MEMD) for investigating magnetospheric and ionospheric current system patterns in the magnetic field data recorded by the Swarm constellation. The aim is to give new insights into the analysis of the different sources responsible of the geomagnetic field of external origin and, at the same time, to provide a filter in the analysis of the geomagnetic field of external origin able to separate the ionospheric signal from both the magnetospheric one and artefacts introduced by unmodeled internal contributions.

2. – Data

In the present study, we use low-resolution (1 Hz) magnetic vector measurements taken on board the Swarm A satellite, one of the three satellites of the Swarm constellation. The selected data cover the time period between 1 April 2014 and 31 March 2016 when the satellite flowed at an average altitude of 470 km with an orbital inclination of 87.30 ° [3]. In detail, we analyze the X and Y components of the geomagnetic field at low and mid-latitudes for two different geomagnetic activity levels: quiet (AE $<$ 80 nT and -10 nT $<$ Sym-H $<$ 5 nT) and disturbed (AE $>$ 100 nT and Sym-H $<$ -40 nT). The Swarm vector magnetometer measurements are in the North-East-Center (NEC) local Cartesian coordinate frame, with the X directed towards geographic North, the Y towards geographic East and Z towards the center of the Earth. The main geomagnetic field and its secular variation and acceleration are removed from the original data using CHAOS-6 geomagnetic field model by using a spherical harmonic expansion up to degree 110. In order to do that, the value of the modeled magnetic fields originated from the core and lithosphere together with the core field temporal variations are estimated at the same location (latitude, longitude and altitude) and at the same time of the Swarm measurement. The residuals, which describe the geomagnetic field of external origin, are presented in terms of the quasi-dipole (QD) coordinate system, which is an apex system, introduced in ref. [4], and organized with respect to the Sun position introducing the local time (LT). Only observations within ($\pm$ 60 °) magnetic latitude are considered. Data are grouped according to their magnetic latitude and LT into 5 ° $\times$ 5 ° bins taking into consideration that a bin size of 5 ° in LT corresponds to a bin size of 20 minutes. Mapped values of the external geomagnetic field along the two magnetic coordinates (X and Y) consist of the averages of the values of the residuals falling in each bin.

3. – Methods: empirical Mode Decomposition (EMD) and its multivariate extension (MEMD)

Time series analysis is usually based on traditional approaches based on Fourier Transform (FT), Lomb-Scargle analysis (LS), Wavelet Transform (WT) [5], while multivariate or multidimensional processes are investigated by using Principal Component Analysis

(PCA) or its variations (*e.g.*, Proper Orthogonal Decomposition (POD), Singular Spectrum Analysis (SSA), Natural Orthogonal Decomposition (NOC), and so on) [6]. Both traditionally univariate and multivariate methods require *a priori* fixed (and usually orthogonal) decomposition basis, also satisfying the mathematical requirement of completeness, formed by linearly independent functions, or linear independent eigenvectors, with most of them also requiring that the signal under investigation must be stationary, like FT or LS [7-9]. In 1998, Huang and co-authors proposed a new time series analysis method, named Hilbert-Huang Transform (HHT), completely removing stationarity and linearity assumptions by using two successive steps: the Empirical Mode Decomposition (EMD) and the Hilbert Spectral Analysis (HSA) [10]. More recently, Rehman and Mandic proposed a multivariate extension of the EMD method to investigate multichannel signals [11]. In the following, we briefly describe both EMD and MEMD methods.

3˙1. *Empirical Mode Decomposition (EMD).* – The EMD is a nonlinear and nonstationary decomposition method which allows to extract an intrinsic oscillating component and embedded structures for time series without any *a priori* assumptions on the functional form of the decomposition basis (*i.e.*, it is a nonlinear self-adaptive decomposition method) [10, 12]. The core of the decomposition is the so-called *sifting process* through which empirical modes are extracted by exploiting intrinsic properties, based on the local extrema of the signal. This process allows to write a signal $x(t)$ as the sum of n empirical modes $c_i(t)$, usually named Intrinsic Mode Functions (IMFs), and a residue $r(t)$, from which no more IMFs can be extracted

$$x(t) = \sum_{i=1}^{n} c_i(t) + r(t). \tag{1}$$

The set of IMFs form the decomposition basis which empirically satisfy all mathematical requirements (*i.e.*, completeness and orthogonality) and, by using the Hilbert Transform, each IMF can be seen as an oscillating component with time-dependent amplitude and frequency, which is the main novelty with respect to the stationary decomposition basis [10, 13]. The EMD has been used in different fields with several purposes: solar activity [14], paleoclimate variations [12], geomagnetic storms and substorms occurrence [15-17, 2, 18], solar wind turbulence [19].

3˙2. *Multivariate Empirical Mode Decomposition (MEMD).* – The Empirical Mode Decomposition (EMD) is particularly suitable when univariate signals are considered, while it cannot be applied to multivariate data. The main problem in applying EMD to multichannel data is that the local mean cannot be computed since, from a theoretical point of view, local extrema cannot be defined for multivariate signals as well as the concept of oscillating modes is rather unknown [11]. Indeed, the main step in extracting IMFs is the computation of the local mean envelope, by averaging upper and lower envelopes defined by local maxima and minima [10]. The first attempts to approach to multivariate signals by using EMD were based on channel-wise processing by applying univariate EMD to each channel [13], with suitable multivariate extensions of EMD only for bivariate and trivariate signals [20, 21]. To perform a suitable n-variate extension of EMD, Rehman and Mandic proposed to generate n-dimensional envelopes by the projection of a multivariate signal along different directions of n-dimensional spaces those extrema are interpolated component-wise to yield the desired multidimensional envelopes of the signal. Then, local mean envelopes are obtained by averaging multiple envelope

curves. The set of direction vectors is chosen by using two different criteria based on uniform angular coordinates and quasi Monte Carlo based low-discrepancy sequences to obtain more accurate local mean estimates in n-dimensional spaces [11].

By defining $\{\mathbf{v}(t)\}|_{t\in T} = \{v_1(t), v_2(t), \ldots, v_n(t)\}$ an n-variate signal, the above procedure can be used to extract a set of k n-dimensional embedded patterns $\{\mathbf{c}_i(t)\}|_{t\in T}^{i=1,\ldots,k}$ such that

$$\{\mathbf{v}(t)\}|_{t\in T} = \sum_{i=1}^{k} \{\mathbf{c}_i(t)\}|_{t\in T} + \{\mathbf{r}(t)\}|_{t\in T}, \tag{2}$$

where $\{\mathbf{c}_i(t)\}|_{t\in T}$ and $\{\mathbf{r}(t)\}|_{t\in T}$ are affine to the i-th IMF $c_i(t)$ and the residue $r(t)$ in eq. (1). A characteristic scale for each MEMD mode can be obtained as $\tau_i = \frac{1}{T}\int_0^T t\langle\{\mathbf{c}_i(t)\}|_{t\in T}\rangle_n \mathrm{d}t$, being $\langle\ldots\rangle_n$ an ensemble average over the n-dimensional space. Moreover, as for EMD, instantaneous amplitudes $\{\mathbf{a}_i(t)\}|_{t\in T}$ and phases $\{\mathbf{\Phi}_i(t)\}|_{t\in T}$ of each MEMD mode can be retrieved by applying the Hilbert Transform over the projection of the multivariate signal along different directions of n-dimensional spaces, and, from instantaneous amplitudes we can derive instantaneous energy contents $\{\mathbf{E}_i(t)\}|_{t\in T}$. By averaging in time and over the n-directions, we can obtain the mean energy associated with each MEMD mode through which relative contributions can be derived as

$$e_i = \frac{\frac{1}{T}\int_0^T t\langle\{\mathbf{E}_i(t)\}|_{t\in T}\rangle_n \mathrm{d}t}{\sum_{i=1}^{k}\frac{1}{T}\int_0^T t\langle\{\mathbf{E}_i(t)\}|_{t\in T}\rangle_n \mathrm{d}t}. \tag{3}$$

Finally, as for EMD modes [10], also MEMD modes empirically satisfy orthogonal and completeness properties [11, 21] in n-dimensional spaces such that partial sums of eq. (2) can be obtained.

In this paper, MEMD will be applied to spatial magnetic measurements (and not to spatio-temporal ones) since the dependence of the magnetic field components on LT does not describe the time evolution of the magnetic measurements but indicates their spatial distribution in the ionosphere with respect to the Sun.

4. – MEMD application to quiet periods

Figure 1 shows magnetic measurements at Swarm altitude of the geomagnetic field of external origin along X (northward) and Y (eastward) components during quiet periods (AE $\leq$ 80 nT and -10 nT $\leq$ Sym-H $\leq$ 5 nT). At low and mid-latitudes, the Swarm vector magnetometer observations of external origin contain contributions from some main sources, such as the ring current, solar quiet daily current (Sq) and equatorial electrojet (EEJ). Among these, the most intense contributions are those of ionospheric origin and consequently those due to the currents flowing in the E-region during daytime, *i.e.* the solar quiet current and the eastward equatorial electrojet. Differently, the auroral electrojets and the field-aligned currents (FACs) represent the most intense ionospheric contributions at higher latitudes.

Figure 1 shows the existence of clear spatial patterns in the equatorial dayside ionosphere. Around 12 LT, a minimum (negative) value is obtained for both X and Y components due to the presence of the equatorial electrojet, while the mid-latitude pattern shows a spatial structure which is compatible to the Sq ionospheric current system (see discussion section) [22, 23]. To gain insights on the above spatial patterns, we applied

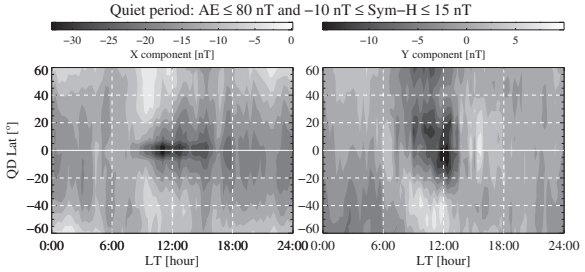

Fig. 1. – X and Y components during quiet periods.

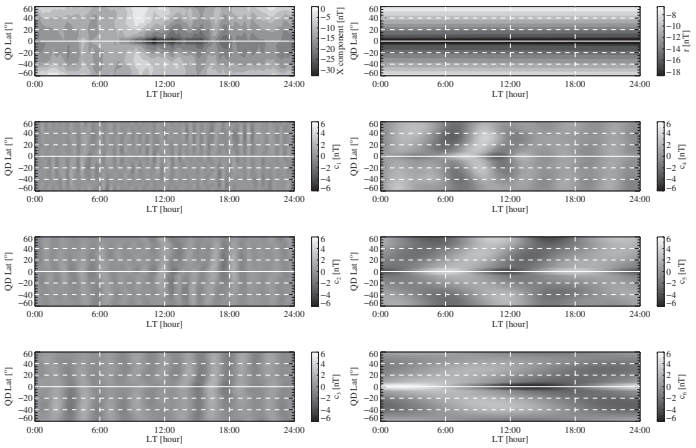

Fig. 2. – MEMD results from X component decomposition during quiet periods.

the MEMD to both X and Y components. In fig. 2 we report the results of the MEMD to the X component for quiet periods.

We obtained a set of $k = 6$ MEMD modes, covering scales τ from minutes up to $\sim$1 day, and a residue with a symmetric behavior in latitude. Short-scale modes (*i.e.*, IMFs 1–3) do not show a well-defined spatial pattern and are characterized by small amplitude variations, while large-scale ones (*i.e.*, IMFs 4–6), exploiting larger amplitude variations, present a characteristic spatial behavior which can be related to the ionospheric current systems. Table I reports for each MEMD mode the characteristic scale in LT and the relative (percentage) contribution to the original signal. According to the different energy contents of MEMD modes, we can reconstruct the original signal using a linear combination of three main contributions: i) a short-scale contribution, based on IMFs 1–3 having a low-energy content ($\sim$2% of the signals), ii) a large-scale reconstruction obtained from IMFs 4–6, representing the main contribution to the signal ($\sim$97%), and iii) the residue. We report these three main patterns in fig. 3.

5. – MEMD application to disturbed periods

Figure 4 presents magnetic field observations along X and Y components during disturbed periods (AE $\geq$ 100 nT and Sym-H ≤ -40 nT). The clear spatial patterns observed during quiet periods are not recovered during disturbed ones. In this case the

TABLE I. – *Characteristic scales in LT τ and relative contributions of each MEMD mode.*

MEMD mode	X component		Y component	
	τ_i (min)	e_i (%)	τ_i (min)	e_i (%)
c_1	50	0.4	51	1.6
c_2	94	0.4	98	0.4
c_3	153	0.8	175	0.5
c_4	281	10.6	463	22.5
c_5	700	31.8	747	51
c_6	1440	56	1230	24

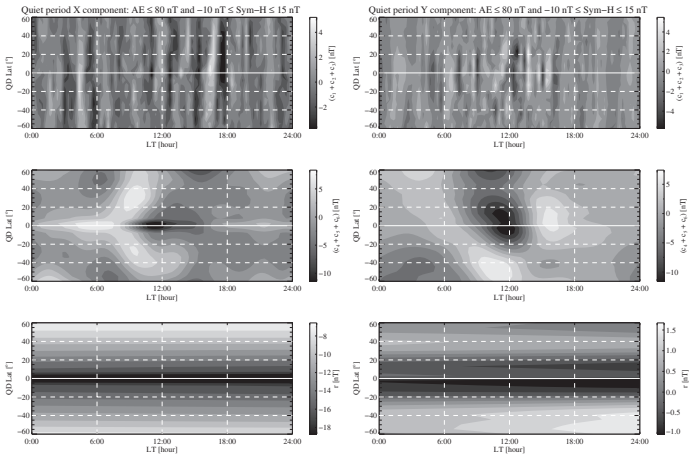

Fig. 3. – MEMD reconstructions during quiet periods: X component (left panels), Y component (right panels).

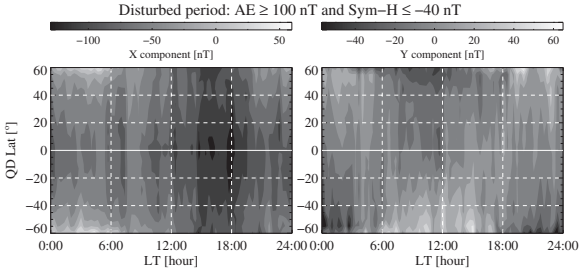

Fig. 4. – X and Y components during disturbed periods.

magnetospheric ring current and field-aligned currents (FACs) are responsible of magnetic variations which are greater than those produced from EEJ and Sq ones. We use, also in this case, the MEMD to investigate spatial patterns in both X and Y components. The results are reported in fig. 5.

We again obtained a set of $k = 6$ MEMD modes, covering scales τ from minutes up to $\sim$1 day, and a residue again with a symmetric behavior in latitude. Short-scale

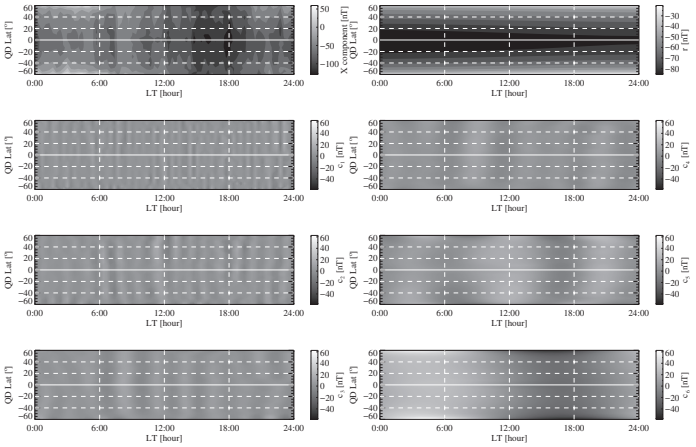

Fig. 5. – MEMD results from X component decomposition during disturbed periods.

modes (*i.e.*, IMFs 1–3) do not show a well-defined spatial pattern, being characterized by an intermittent-like behavior and by small amplitude variations, while large-scale ones (*i.e.*, IMFs 4–6 on scales in LT of ∼4, 6, and 24 hours) present a well-structured larger amplitude spatial behavior. For each MEMD mode the characteristic scale in LT and the relative (percentage) contribution to the original signal are reported in table II. According to the different energy contents of MEMD modes, we can reconstruct the original signal using a linear combination of three main contributions: i) a short-scale contribution, based on IMFs 1–5 having low-energy content (∼3% of the total original signal), ii) a large-scale reconstruction obtained from IMFs 6, representing the main contribution to the original signal (∼97%), and iii) a residue. The main spatial patterns recognized in the original signal by the MEMD method are shown in fig. 6.

6. – Discussion

The results of this study indicate that a few modes (*i.e.*, IMFs 4–6) are necessary to reconstruct spatial patterns which are related to the EEJ and the Sq currents, in the

TABLE II. – *Characteristic scales in LT τ and relative contributions of each MEMD mode.*

MEMD mode	X component		Y component	
	τ_i (min)	e_i (%)	τ_i (min)	e_i (%)
c_1	52	0.2	50	1.5
c_2	90	0.2	97	0.2
c_3	160	0.1	160	1.0
c_4	243	0.1	346	0.2
c_5	501	0.6	639	0.1
c_6	1420	98.2	1440	97

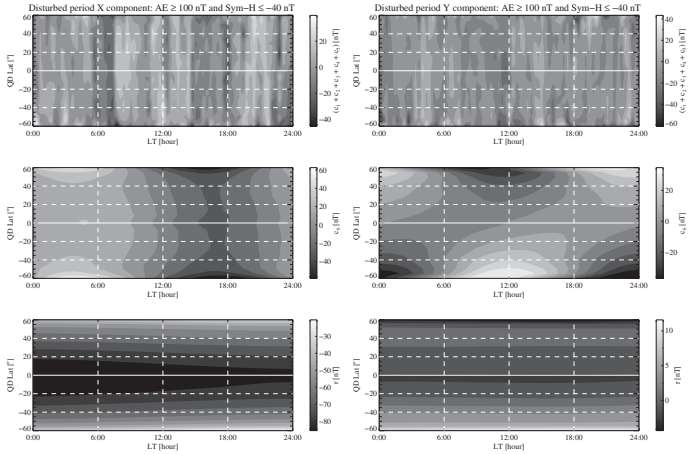

Fig. 6. – MEMD reconstructions during disturbed periods: X component (left panels), Y component (right panels).

magnetic field data recorded during quiet periods (see figs. 1–3). Indeed, moving from north to south, both Sq and EEJ are encountered. In detail, Sq, whose effects are visible on the magnetic field measurements during geomagnetically "quiet" period and depend on solar (local) time, is expected to produce magnetic variations on the order of a few tens of nanotesla on the ground. This current system, which arises from thermal-tidal motions in the E-region of ionosphere, is formed by two vortices, one in each hemisphere, fixed with respect to the Earth-Sun line. Viewed from the above ionosphere, in the Northern Hemisphere the vortex is counterclockwise, while in the Southern Hemisphere it is clockwise. This means that along the X component, the Sq current system produces an external magnetic field characterized by negative values at low latitudes and positive at higher ones near midday. The pattern tends to be symmetric with respect to the magnetic equator. Along the eastward (Y) component, Sq is responsible of a recurring pattern at all latitudes in the Northern Hemisphere which is due to two different directions of the current: southward at the first part of the day and northward in the afternoon [24-28]. Along the X component it is also possible to see a small structure probably associated with the EEJ. This eastward ionospheric current is responsible of the large decrease in the X component of the external magnetic field that reaches the maximum value around local noon. This strong zonal current, which is driven by the solar-wind magnetospheric dynamo, is located within the narrow band of 3° over the magnetic equator in the dayside ionosphere. It is characterized by a non-uniform strength which is weakened during the early morning and evening. All these features are captured by the main pattern obtained from the linear combination of large-scale modes ($\tau \geq 4$ hours, *i.e.*, IMFs 4–6). Moreover, the characteristic scales of IMFs 4–6 can be related to the different sources/periodicities of Sq and EEJ ionospheric current systems. Indeed, the main driver of the Sq current is the external tidal wave mode which shows both a semidiurnal and a diurnal component, phase shifted by 180 ° [29, 30, 23, 31, 16]. This is the result of the nonlinear coupling between the diurnally varying wind and conductivity, showing a day-to-day variability. During disturbed periods, a clear spatial pattern associated with the Sq and/or the EEJ is not seen. Indeed, in this case, the magnetic field behavior is influenced by the ring and magnetopause current activity at noon, while at midnight the superimposed effect

of the ring and tail currents can be seen. During quiet periods magnetic variations are principally due to the Sq and EEJ contributions (∼97%), while during disturbed periods, these two ionospheric current systems have less weight. Indeed, the interaction between solar wind and magnetosphere is responsible for increasing the intensity of the electric currents due to solar wind particle entering the magnetosphere. These currents generate intense magnetic fields which are the main responsible of external variations of the geomagnetic field. This can be clearly evidenced by looking at figs. 4–6 from which the dominant spatial pattern is probably due to the partial ring current on the night side. Moreover, high-latitude magnetic field variations, characterized by two vortex of opposite polarity, can be also seen from fig. 6. This is related to the auroral electrojets enhancements via field-aligned currents (FACs) activity.

7. – Conclusions

In this paper an application of the Multivariate Empirical Mode Decomposition (MEMD) has been proposed to investigate geomagnetic field variations of external origin and to detect ionospheric and magnetospheric current systems patterns. By using magnetic Swarm A data and by discerning between quiet and disturbed periods, we found that, during quiet periods the MEMD method is able to reconstruct the spatial pattern describing the Sq and EEJ variations by using only three MEMD modes (with scales between 4 and 24 hours). During disturbed periods the main external contributions to the geomagnetic field can be reconstructed using only one mode.

The first modes, which we have found analyzing both quiet and disturbed periods, are probably due to an artifact introduced by CHAOS 6 geomagnetic field model used to extract the external contributions from the total magnetic measurements. The rapid time-varying magnetic fluctuations along the satellite track used in the model are indeed misinterpreted as spatial variations of the static lithospheric field. North-South patterns like those observed in the first IMFs can be consequently interpreted as a noise in the analyzed magnetic data.

At the end, the residual signals, which we have found in our analysis describing the part of the original signal that cannot be decomposed into IMFs, represent important contributions to our decomposition being of the same order of the analyzed signal. Considering their spatial structures and their increase in the intensity according to the geomagnetic activity level, we can suppose that they are consistent with the contribution expected from the westward ring current.

* * *

The results presented in this paper rely on magnetic data, collected by the ESA-Swarm mission, freely available in .cdf file format at `ftp://swarm-diss.eo.esa.int` upon registration. We thank the European Space Agency that supports the Swarm mission. The author kindly thanks P. De Michelis and F. Giannattasio, at Istituto Nazionale di Geofisica e Vulcanologia (INGV), for providing elaborated data and for valuable and helpful discussions and comments, and G. Consolini, at INAF-Istituto di Astrofisica e Planetologia Spaziali (IAPS), for valuable and fruitful discussions and suggestions.

REFERENCES

[1] Merrill R. T., McElhinny M. W. and McFadden P. L., *Magnetic Field of the Earth: Paleomagnetism, the Core and the Deep Mantle* (Academic, San Diego) 1996.

[2] Alberti T., Consolini G., Lepreti F., Laurenza M., Vecchio A. and Carbone V., *J. Geophys. Res.*, **122** (2017) 4266.
[3] Olsen N., Friis-Christensen E., Floberghagen R. *et al.*, *Earth Planets Space*, **65** (2006) 1189.
[4] Richmond A. D., *J. Geomagn. Geoelectr.*, **47** (1995) 191.
[5] Chatfield C., *The Analysis of Time Series: An Introduction, 6th edition* (Chapman and Hall/CRC, London) 2016, pp. 352.
[6] Chatfield C. and Collins A. J., *Principal component analysis*, in *Introduction to Multivariate Analysis* (Springer, Boston, MA) 1980, pp. 57–81.
[7] Brillinger D. R., *Proc. IEEE*, **62** (1974) 1628.
[8] Lomb N. R., *Astrophys. Space Sci.*, **39** (1976) 447.
[9] Scargle J. D., *Astrophys. J.*, **263** (1982) 835.
[10] Huang N. E., Shen Z., Long S. R. *et al.*, *Proc. R. Soc. Lond. A*, **454** (1998) 903.
[11] Rehman N. and Mandic D. P., *Proc. R. Soc. Lond. A*, **466** (2010) 1291.
[12] Alberti T., Lepreti F., Vecchio A., Bevacqua E., Capparelli V. and Carbone V., *Clim. Past*, **10** (2014) 1751.
[13] Huang N. E. and Wu Z., *Rev. Geophys.*, **46** (2008) RG2006.
[14] Vecchio A., Lepreti F., Laurenza M., Alberti T. and Carbone V., *Astron. Astrophys.*, **599** (2017) A58.
[15] De Michelis P., Consolini G. and Tozzi R., *Nonlinear Proc. Geophys.*, **19** (2012) 667.
[16] Alberti T., Piersanti M., Vecchio A., De Michelis P., Lepreti F., Carbone V. and Primavera L., *Ann. Geophys.*, **34** (2016) 1069.
[17] De Michelis P., Tozzi R. and Consolini G., *Earth Planets Space*, **69** (2017) 24.
[18] De Michelis P., Consolini G., Tozzi R. and Marcucci M. F., *J. Geophys. Res.*, **122** (2017) https://doi.org/10.1002/2017JA024156.
[19] Consolini G., Alberti T., Yordanova E., Marcucci M. F. and Echim M., *J. Phys.: Conf. Ser.*, **900** (2017) 012003.
[20] Rilling G., Flandrin P., Goncalves P. and Lilly J. M., *IEEE Signal Process. Lett.*, **14** (2007) 936.
[21] Rehman N. and Mandic D. P., *IEEE Trans. Signal Process.*, **58** (2010) 1059.
[22] Chapman S., *Proc. R. Soc. Lond. Ser. A*, **129** (1929) 369.
[23] De Michelis P., Tozzi R. and Consolini G., *Ann. Geophys.*, **28** (2010) 2213.
[24] Richmond A. D., Matsushita S. and Tarpley J. D., *J. Geophys. Res.*, **81** (1976) 547.
[25] Reddy C. A., *Pure Appl. Geophys.*, **131** (1989) 485.
[26] Stening R. J., *Ann. Geophys.*, **26** (2008) 1767.
[27] Yamazaki Y. and Yumoto K., *Earth Planets Space*, **64** (2012) 417.
[28] Shinbori A., Koyama Y., Nose M., Hori T., Otsuka Y. and Yatagai A., *Earth Planets Space*, **66** (2014) 155.
[29] Feldstein Y. I. and Zaitzev A. N., *Tellus*, **20** (1968) 338.
[30] Dominici P., Cander L. R. and Zolesi B., *Ann. Geophys.*, **40** (1997) 5.
[31] Fytterer T., Arras C. and Jacobi C., *Adv. Radio Sci.*, **11** (2013) 333.